

III–V selective regrowth on SOI for telecom lasers in silicon photonics

Cite as: J. Appl. Phys. **133**, 133103 (2023); <https://doi.org/10.1063/5.0144377>

Submitted: 29 January 2023 • Accepted: 22 March 2023 • Published Online: 06 April 2023

 Jie Li,  Ying Xue,  Zhao Yan, et al.



View Online



Export Citation



CrossMark

ARTICLES YOU MAY BE INTERESTED IN

[Heterogeneous integration of III–V semiconductor lasers on thin-film lithium niobite platform by wafer bonding](#)

Applied Physics Letters **122**, 081103 (2023); <https://doi.org/10.1063/5.0142077>

[Perspective on the future of silicon photonics and electronics](#)

Applied Physics Letters **118**, 220501 (2021); <https://doi.org/10.1063/5.0050117>

[Soliton trains induced by femtosecond laser filamentations in transparent materials with saturable nonlinearity](#)

Journal of Applied Physics **133**, 133102 (2023); <https://doi.org/10.1063/5.0139398>



Time to get excited.
Lock-in Amplifiers – from DC to 8.5 GHz

[Find out more](#)

 Zurich
Instruments

III–V selective regrowth on SOI for telecom lasers in silicon photonics

Cite as: J. Appl. Phys. **133**, 133103 (2023); doi: [10.1063/5.0144377](https://doi.org/10.1063/5.0144377)

Submitted: 29 January 2023 · Accepted: 22 March 2023 ·

Published Online: 6 April 2023



View Online



Export Citation



CrossMark

Jie Li,¹ Ying Xue,¹ Zhao Yan,¹ Yu Han,¹ and Kei May Lau^{1,2,a)}

AFFILIATIONS

¹Department of Electronic and Computer Engineering, The Hong Kong University of Science and Technology, Clear Water Bay, Kowloon, Hong Kong

²Department of Electronic Engineering, The Chinese University of Hong Kong, Shatin, Hong Kong

^{a)}Author to whom correspondence should be addressed: eeekmlau@ust.hk and kmlau@ee.cuhk.edu.hk. Tel.: (852) 23587049.

Fax: (852) 23581485.

ABSTRACT

To realize fully integrated silicon photonics (Si photonics), reliable III–V light sources that can be efficiently coupled with Si/SiN waveguides are essential. Here, based on a monolithic InP/silicon-on-insulator (SOI) platform, we developed a selective regrowth scheme and constructed a regrowth platform for on-chip lasers that can be efficiently coupled with Si/SiN waveguides. InP and InGaAs/InP multi-quantum wells (MQWs) were regrown on the regrowth template on SOI as well as patterned commercial InP wafers in the same growth run for comparison. A flat (001) top surface after regrowth with a low roughness of 0.38 nm was obtained on SOI. Benefitting from the high quality of MQWs regrowth, strong photoluminescence emission at telecom band can be obtained on both growth templates. Also, multi-wavelength emission on the same chip can be potentially achieved by designing various regrowth openings. Furthermore, the large material volume with vertical stacking structure and intimate placement of MQWs and the Si layer of SOI allow for the potential demonstration of electrically pumped lasers and efficient light coupling between them and Si/SiN waveguides. Therefore, the demonstrated regrowth method provides a promising solution for the monolithic integration of III–V on-chip lasers on Si.

Published under an exclusive license by AIP Publishing. <https://doi.org/10.1063/5.0144377>

I. INTRODUCTION

In recent years, the rapid growth of Internet data traffic calls for data transmission with higher speed and larger throughput. Photonic integrated circuits (PICs) are revolutionizing data communication by replacing conventional electrical wires with faster optical interconnects.^{1,2} Leveraging on the mature complementary metal-oxide-semiconductor (CMOS) technology, silicon photonics (Si photonics) has attracted a great deal of interest because of its low cost, high bandwidth capacity, and large scalability.^{3,4} However, reliable III–V on-chip lasers on Si remain the last missing piece in the puzzle of fully integrated Si photonics.^{5–7} Heterogeneous integration using bonding and transfer printing techniques^{8–10} has been extensively investigated and commercialized for lasers on Si. Alternatively, monolithic integration via direct epitaxy provides a solution for fully integrated Si photonics in a manner with potentially lower cost and larger scalability.¹¹

Monolithic integration of III–V lasers on Si using blanket epitaxy has witnessed notable success with impressive device results in the past decade.^{12–15} However, the micrometer-thick

buffer needed for defect reduction makes the light coupling between the III–V and Si challenging. As an alternative, using the unique defect necking effect,¹⁶ selective epitaxy can generate dislocation-free III–V materials on Si without thick buffers. Conventional selective growth methods^{17–24} usually grow nanometer-scale III–V on Si, on which optically pumped nano-lasers emitting at O-band and C-band and nano-photodetectors have been realized.^{25–31} However, the limited material volume makes the demonstration of electrically pumped lasers challenging. In contrast, III–V crystal grown by the lateral aspect ratio trapping (LART) method features a material dimension over tens of or even hundreds of micrometers. In previously reported work, we have demonstrated 920 nm lasers, 1.55 μm micro-lasers, high-performance photodetectors, and efficient light coupling between III–V photodetectors and Si waveguides by adopting the LART on the InP/silicon-on-insulator (SOI) platform.^{32–35} Whereas, the electrically pumped laser has yet to be reported due to the lateral “stacking” of the full laser structure adds complexity to the device design and growth.

Here, we demonstrated InP and InGaAs/InP multi-quantum wells (MQWs) grown on SOI by adopting a regrowth technique for the monolithic integration of on-chip lasers. The regrowth template was fabricated by defining disk and stripe regrowth openings on the monolithic InP/SOI platform.³² Patterned commercial InP wafers with the same regrowth openings were put in the same run and used as growth references. Starting from InP regrowth, the regrown thickness can be as thin as 80 nm with a smooth surface evidenced by a low roughness of 0.38 nm, which enables intimate placement of the III–V and Si. Then, we further incorporated four periods of InGaAs/InP MQWs to achieve the telecom band emission. The regrown MQWs display strong room temperature (RT) micro-photoluminescence (μ -PL) emission at telecom band resulting from the high III–V crystalline quality without observable dislocations. We also studied and compared the emission wavelength and regrowth thickness on different regrowth openings. The bufferless structure, large material volume, and vertically stacked active region suggest a high potential of realizing electrically pumped lasers and efficient light coupling between III–V and Si waveguides.

II. REGROWTH SCHEME

We built up the regrowth template for vertical regrowth starting from a monolithic InP/SOI platform containing InP segments

with a 7- μm width and flexible lengths ranging from 5 to 50 μm [Figs. 1(a) and 1(b)] defined by lithography. Commercial (001) SOI wafers were used for lateral InP growth, and the (001) top surface of the lateral grown InP features a low roughness with a roughness value of 0.27 nm [Fig. 2(e)]. The detailed growth procedure was discussed in Ref. 32. The laterally grown InP features a high crystalline quality which is free of threading dislocations, antiphase boundaries, and grain boundaries with a zinc-blende crystal phase. The process for fabricating the regrowth template is as follows. The top low-temperature oxide (LTO) on the InP/SOI platform was first etched down to around 50 nm. Then, 500 nm thick plasma-enhanced chemical vapor deposition (PECVD) oxide was deposited to cover the InP end and provide sufficient depth for the regrowth opening. Therefore, the III–V material can only be grown vertically from the (001) top facet of the InP instead of the (111) facet at the InP end during the regrowth. After the oxide encapsulation, regrowth openings with various dimensions and shapes were defined on the template using photolithography and combined dry etching and wet etching steps. Benefiting from the combined etching process, the slope of the oxide opening was minimized, and the damage to the III–V surface for regrowth was eliminated. Both disk regrowth openings with a diameter of 4 μm and stripe regrowth openings with a width of 4 μm and lengths ranging from 5 to 50 μm were defined on the InP/SOI platform to demonstrate the viability of the regrowth technique [Fig. 1(a)]. Regrowth

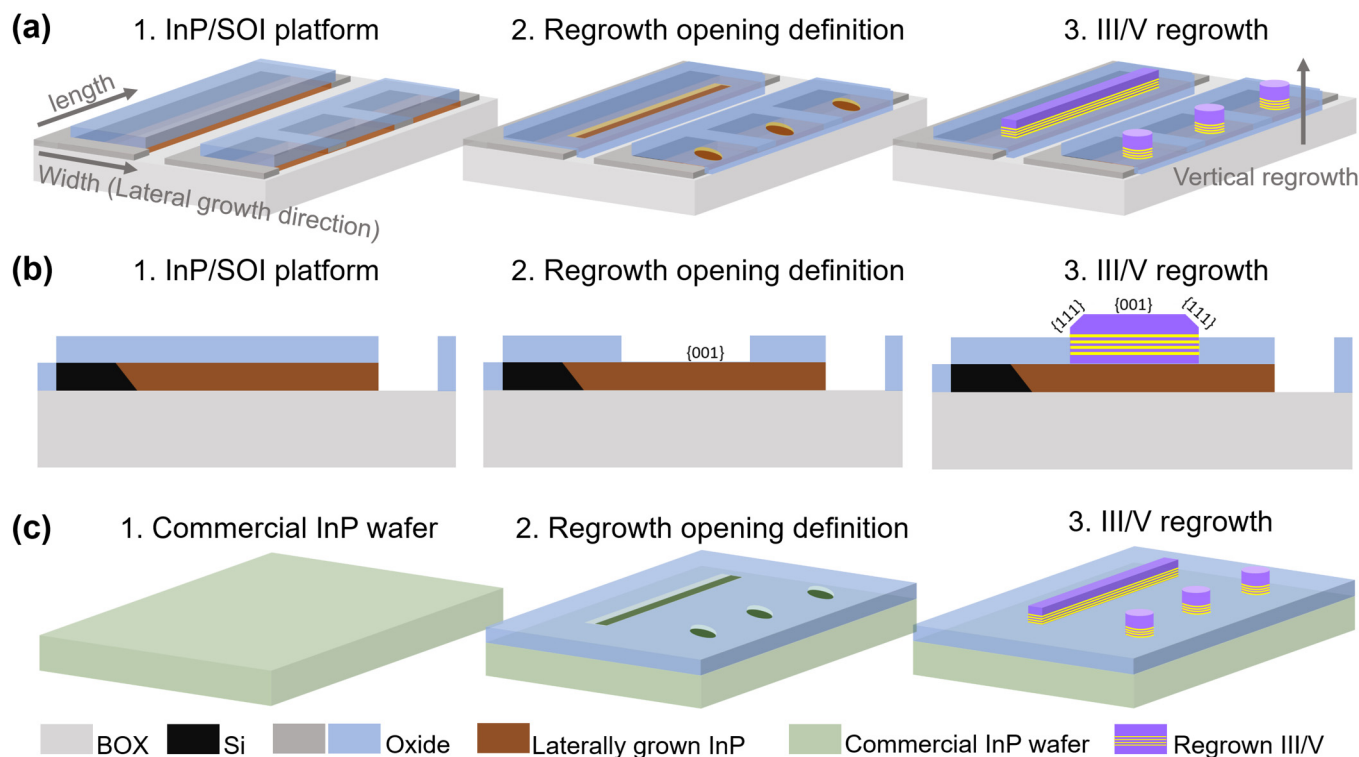


FIG. 1. (a) Regrowth scheme on the regrowth template on SOI. (b) Cross-sectional schematic of one regrowth opening on the regrowth template on SOI. (c) Regrowth scheme on the patterned commercial InP wafer.

(001) facet will orientate the crystal with an upper (001) facet surrounded by four {111} planes and four {110} planes as sidewalls, labeled in Fig. 2(b). Surface smoothness after the InP regrowth was further evidenced by the low root mean square (RMS) value of 0.38 and 0.312 nm on the regrowth template on SOI and patterned commercial InP wafer, respectively, as presented in Figs. 2(f) and 2(h). Compared with the InP/Si template by traditional blanket epitaxy with the surface roughness of 2.8 nm,¹² the regrowth template on SOI in this work features a lower surface roughness of only 0.38 nm.

To close the MQWs and the Si device layer for efficient light coupling, the thickness of the regrown InP was further decreased. We adopted a two-step regrowth procedure including a 25 nm/min high-rate growth at the beginning to fastly smoothen the regrowth interface and a subsequent 5 nm/min low-rate growth to facilitate the precise control of the regrowth thickness. By adopting the two-step regrowth procedure, the thickness of regrown InP can be reduced tenfold from 800 to 80 nm, as estimated from cross-sectional view SEM photos in Figs. 3(c) and 3(d). Tiny dots on the regrown InP surface in Fig. 3(d) were caused by the ion damage during focused ion beam (FIB) cutting. Note that the 80 nm regrown InP surface remains smooth as compared in Figs. 3(a) and 3(b). We also performed RT μ -PL measurement to further investigate the crystalline quality of the regrown InP. For all μ -PL measurements in this work, we used a 514 nm laser diode as the excitation source with a pumping power of 6.25 mW. The PL measured on the regrown InP on the regrowth template on SOI presents a FWHM of 50 meV [Fig. 3(e)] which is slightly higher than that measured on the patterned commercial InP wafer. The relatively larger FWHM on the regrowth template on SOI can be attributed to the crystalline defects in the laterally grown InP/SOI template, including SFs perpendicular to the growth direction and the highly twinned InP/Si interface. The red-shifted central

wavelength on the InP/SOI regrowth template is caused by background impurities incorporated during the lateral epitaxy, which creates recombination centers with reduced bandgap energy.⁴⁴

IV. REGROWTH OF InGaAs/InP MQWS

Based on the uniform InP regrowth, we further incorporated InGaAs/InP MQWs to achieve telecom band emission. As depicted in the growth structure and growth sequence in Figs. 4(b) and 4(d), four periods of InGaAs/InP MQWs were regrown on two templates under 620 °C, sandwiched by 200 nm bottom InP cladding and 200 nm top InP cladding. The growth parameter of InP was kept the same as the pre-optimized condition to provide a smooth growth front for subsequent QW deposition. Figure 4(c) illustrates the cross-sectional transmission electron microscopy (TEM) lamella prepared on one segment with disk regrowth opening after MQWs regrowth [Fig. 4(a)]. From the global-view TEM photo in Fig. 4(c), the as-grown MQWs display high crystalline quality without observable dislocations resulting from the bottom dislocation-free InP/SOI platform and well-optimized vertical regrowth. QWs at the center region were generally uniformly distributed. At the edge region of the regrowth opening, closing to the InP/Si interface, the uniformity of QWs is degraded by the defective region near the InP/Si interface. Also, the growth rate on the edge region was also significantly enhanced by the edge-enhancement growth mode and loading effect. In order to get more uniform QWs regrowth with higher quality and better optical property, the crystalline quality of the laterally grown InP/SOI template and the regrowth condition can be further optimized. The thickness of each layer matches well with what we design in Fig. 4(b). Benefiting from the well-developed regrowth template and growth conditions, there is no observable defect at the regrowth interface from Fig. 4(g), allowing for the subsequent

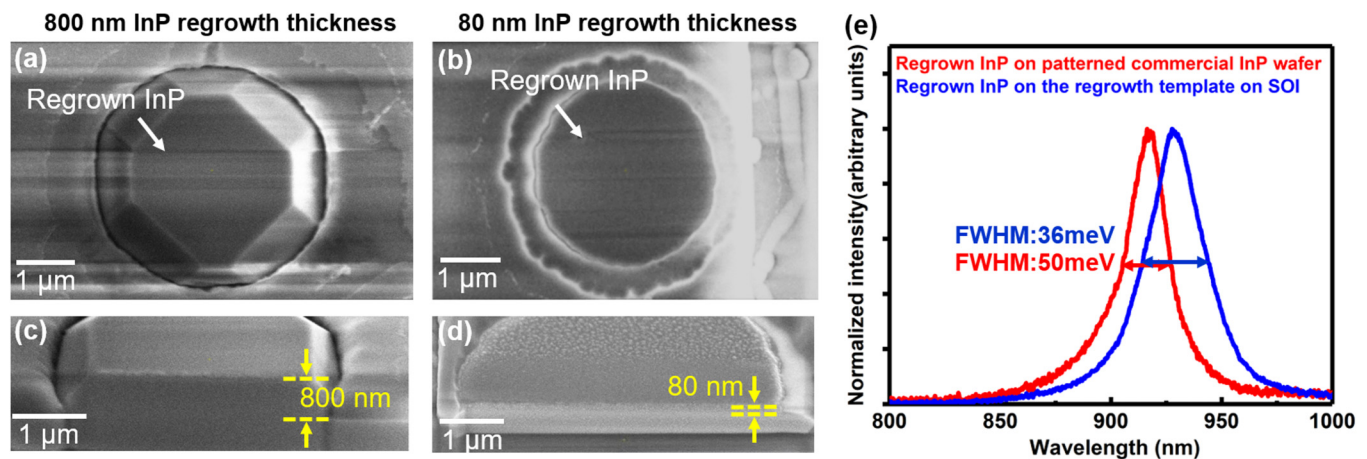


FIG. 3. (a) Top-view SEM image of 800 nm regrown InP on the regrowth template on SOI. (b) Top-view SEM image of 80 nm regrown InP on the regrowth template on SOI. (c) Cross-sectional SEM image of 800 nm regrown InP on the regrowth template on SOI after FIB cutting. (d) Cross-sectional SEM images of 80 nm regrown InP on the regrowth template on SOI after FIB cutting. (e) Normalized RT μ -PL spectra of 800 nm regrown InP on the regrowth template on SOI and patterned commercial InP wafer.

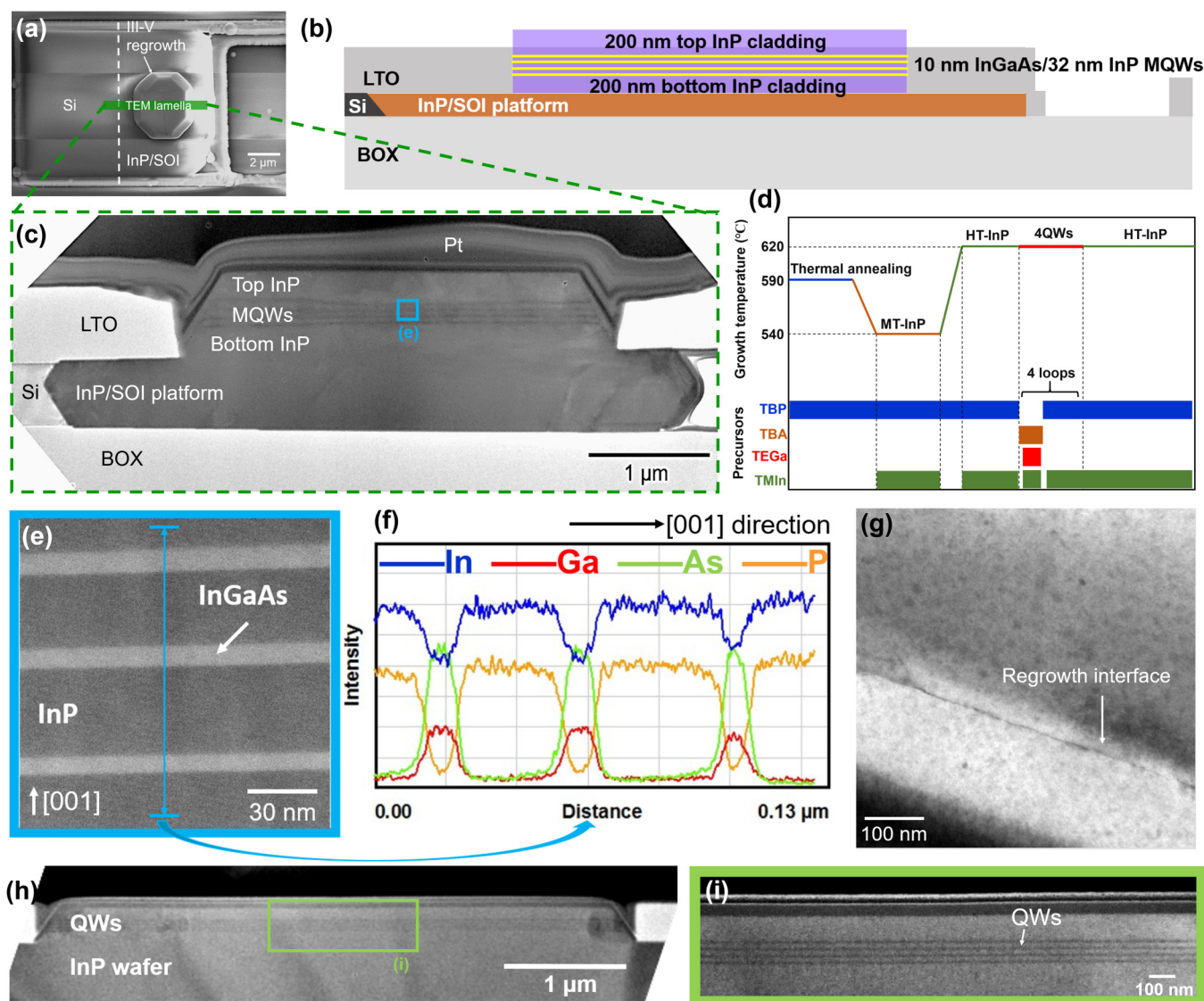


FIG. 4. (a) Top-view SEM image of one segment after MQWs regrowth with disk regrowth opening for TEM characterization. (b) Growth structure of four periods of InGaAs/InP MQWs on the regrowth template on SOI. (c) Global-view TEM image of MQWs regrown on the regrowth template on SOI. (d) Growth sequence of four periods of InGaAs/InP MQWs regrowth. (e) Zoomed-in STEM photo of uniform QWs stacking on the regrowth template on SOI. (f) The indium, gallium, arsenic, and phosphorus intensity against distance along the [001] direction obtained by EDS line scanning. (g) Zoomed-in TEM image of the regrowth interface without defect. (h) Global-view TEM image of MQWs regrown on the patterned commercial InP wafer. (i) Zoomed-in TEM photo of uniform QWs stacking on the patterned commercial InP wafer.

epitaxy of high-quality QWs. The high-quality III-V regrowth was also evidenced by the flat (001) top surface without surface pits in Fig. 4(c). The InGaAs well thickness and indium composition were further analyzed by cross-sectional scanning transmission electron microscopy (STEM) observation. The evenly spaced 10-nm InGaAs well displays a sharp interface with the 35-nm InP barrier, as displayed in Fig. 4(e). To characterize the elemental distribution along

the [110] direction in the QW region (follow the blue double arrow line), four energy dispersive spectrometry (EDS) line scanning curves regarding indium, gallium, arsenic, and phosphorus intensity were performed and summarized in Fig. 4(f). From the relative intensity of EDS signals, the indium composition in InGaAs well was calculated to be 65%, indicating the MQWs to be somewhat compressively strained. The QWs regrown on the

patterned commercial InP wafer were characterized and displayed in Fig. 4(h). The majority of QWs feature high uniformity and evenly spaced stacking as shown in Fig. 4(i), while the edge region of the QWs was somewhat affected by the loading effect.

Figures 5(a)–5(c) and 5(d)–5(f) compare the surface morphology after the MQW regrowth on two templates in the same growth run. We obtained a smooth surface on both small disk regrowth openings with $4\ \mu\text{m}$ diameter and larger stripe regrowth openings with $4\ \mu\text{m}$ width and variable lengths from 5 to $50\ \mu\text{m}$. The regrowth technique shows the versatility of obtaining large growth areas with different shapes and dimensions, allowing for diverse structural and cavity designs as well as providing sufficient material volume for electrically pumped lasers in the future. Note that the more evolution of regrown structures on the regrowth template on SOI stems from the relatively higher growth rate on it. The III–V crystal regrown out of the oxide pocket will lose the confinement of the sidewall oxide, thereby intensifying the growth preference on $\{111\}$ facets. The representative RT μ -PL

spectra of MQWs on the regrowth template on SOI and the patterned commercial InP wafer are displayed in Fig. 5(g), showing strong emission at telecom band. The representative emission wavelength of MQWs regrown in $20\ \mu\text{m}$ long stripes on the patterned commercial InP wafer and the regrowth template on SOI is 1480 and 1560 nm, respectively. The resonance peaks in the spectra may be caused by the natural cavities formed by the as-grown III–V crystals with smooth and symmetric sidewalls. PL emission wavelength as well as regrowth thickness vs regrowth area are plotted in Fig. 5(h). The emission wavelength, determined by the thickness of the InGaAs well, can be tuned by changing the regrowth area on the same chip. Therefore, the selective regrowth technique is promising to potentially provide multi-wavelength lasers on the same chip for multi-channel communications. This is enabled by the unique selective regrowth technique using a larger regrowth opening associated with a slower growth rate, thereby a thinner well and shorter emission wavelength. Data obtained on the regrowth template on SOI and

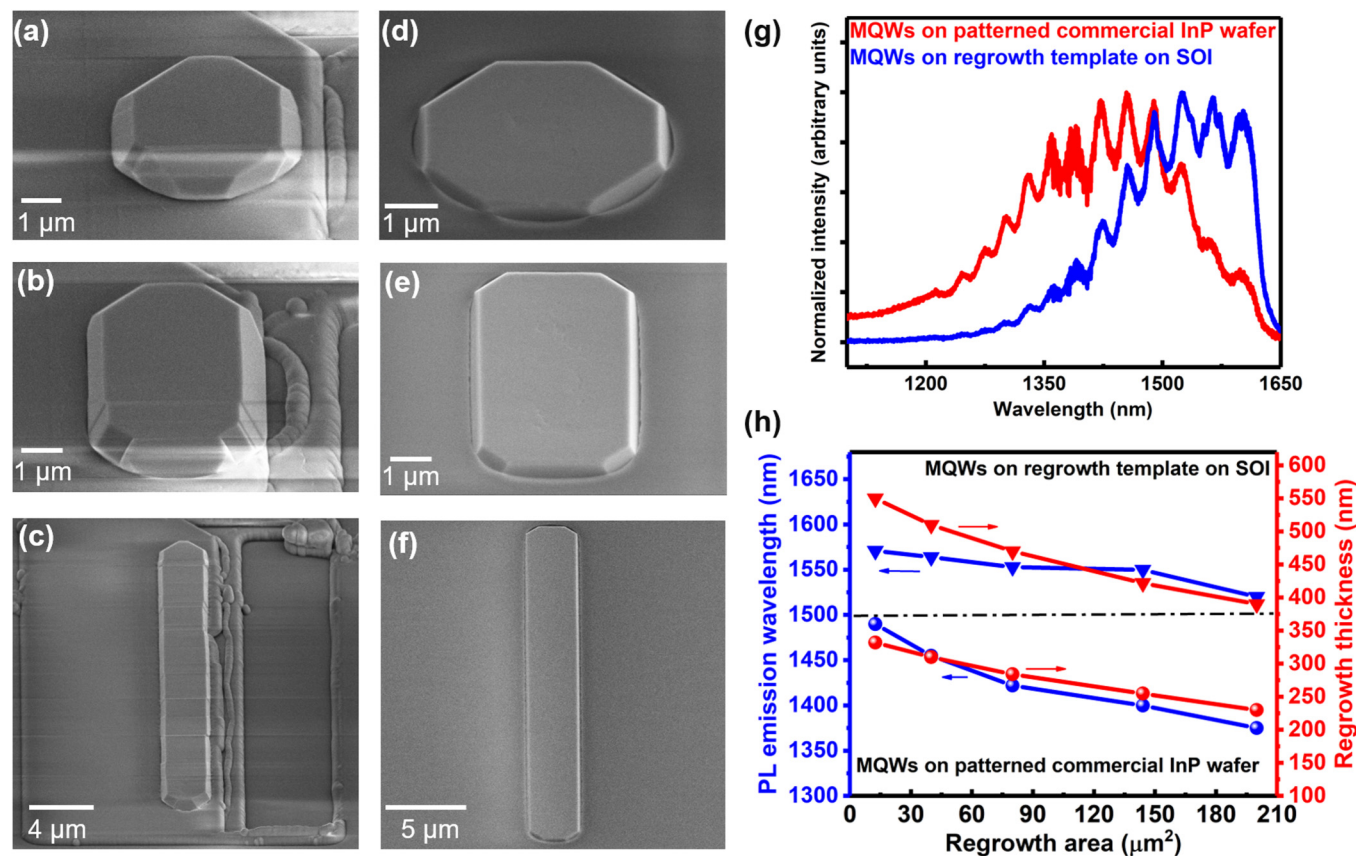


FIG. 5. Tilted view SEM images after MQWs regrowth on the regrowth template on SOI with (a) disk regrowth opening of $3\ \mu\text{m}$ diameter, (b) stripe regrowth opening of $10\ \mu\text{m}$ length, and (c) stripe regrowth opening of $36\ \mu\text{m}$ length. Tilted view SEM images after MQWs regrowth on the patterned commercial InP wafer with (d) disk regrowth opening of $3\ \mu\text{m}$ diameter, (e) stripe regrowth opening of $10\ \mu\text{m}$ length, and (f) stripe regrowth opening of $36\ \mu\text{m}$ length. (g) RT μ -PL spectra of MQWs regrowth on the regrowth template on SOI and the patterned commercial InP wafer on $20\ \mu\text{m}$ long stripe. (h) PL emission wavelength and regrowth thickness against the regrowth area on the regrowth template on SOI and the patterned commercial InP wafer.

patterned commercial InP wafer follow the similar trend. The higher regrowth rate was observed on the regrowth template on SOI, which is caused by the higher epi true temperature and larger deposition amount on the thicker SOI wafer.

The regrowth strategy on the InP/SOI platform provides a promising solution for monolithic integration of III–V on Si. As a thin InP layer can be grown on the regrowth template on SOI with excellent crystalline quality, the distance between III–V active media and Si device layer was minimized which is the key to efficient coupling. Electrically pumped lasers and their integration with Si/SiN-based passive components can be potentially realized with a similar structure to those demonstrated by bonding-based techniques. Also, we can easily transfer the fabrication techniques and structural designs that have been developed for years on InP-based PICs benefiting from the similar vertical structures.^{45,46} Distributed feedback lasers, amplifiers, and photodetectors can be demonstrated on this platform to provide various functionalities. Furthermore, we can also incorporate quantum dots (QDs) to improve the device performance benefiting from the flat (001) facet in the selective regrowth template which is not available in other selective growth schemes.

V. CONCLUSIONS

In conclusion, we demonstrated the regrowth technique on a monolithic InP/SOI platform. Disk and stripe regrowth openings with flexible dimensions were defined on the InP/SOI platform as well as commercial InP wafers, on which we grew InP and InGaAs/InP MQWs for emission at the telecom band. A smooth surface with the surface roughness of 0.38 nm was obtained after regrowth, and good optical characteristics with a strong emission at telecom band were both achieved on the regrowth template on SOI and patterned commercial InP wafer. The regrown InP can be as thin as 80 nm, leading to an intimate placement of III–V gain and Si device layer for efficient light coupling between them. The vertical structure with flexible dimensions also allows for various designs of devices and multi-wavelength emission on the same chip. These results verified the selective regrowth template on SOI as a promising platform to realize electrically pumped lasers for fully integrated Si photonics.

ACKNOWLEDGMENTS

This study was funded by Research Grants Council, University Grants Committee (No. 16213420) and Innovation and Technology Fund (No. ITS/226/21FP). The author would like to acknowledge Nanosystem Fabrication Facility (NFF) and Material Characterization and Preparation Facility (MCPF) of HKUST for their technical support. Fruitful discussions with Jie Huang, Wei Luo, and Ka Ming Wong are also acknowledged.

AUTHOR DECLARATIONS

Conflict of Interest

The authors have no conflicts to disclose.

Author Contributions

J.L. and Y.X. contributed equally to this work.

Jie Li: Conceptualization (equal); Data curation (lead); Investigation (lead); Methodology (lead); Writing – original draft (lead); Writing – review & editing (lead). **Ying Xue:** Conceptualization (equal); Data curation (lead); Investigation (lead); Methodology (lead); Supervision (equal); Writing – review & editing (lead). **Zhao Yan:** Data curation (supporting); Investigation (supporting); Methodology (supporting); Supervision (supporting); Writing – review & editing (supporting). **Yu Han:** Conceptualization (supporting); Data curation (supporting); Supervision (supporting); Writing – review & editing (supporting). **Kei May Lau:** Conceptualization (lead); Project administration (lead); Supervision (lead); Writing – review & editing (lead).

DATA AVAILABILITY

The data that support the findings of this study are available from the corresponding author upon reasonable request.

REFERENCES

- ¹M. Haurylau, G. Chen, H. Chen, J. Zhang, N. A. Nelson, D. H. Albonese, E. G. Friedman, and P. M. Fauchet, *IEEE J. Sel. Top. Quantum Electron.* **12**, 1699 (2006).
- ²J. W. Goodman, F. J. Leonberger, S. Y. Kung, and R. A. Athale, *Proc. IEEE* **72**, 850 (1984).
- ³D. Thomson, A. Zilkie, J. E. Bowers, T. Komljenovic, G. T. Reed, L. Vivien, D. Marris-Morini, E. Cassan, L. Virot, J. M. Fédéli, J. M. Hartmann, J. H. Schmid, D. X. Xu, F. Boeuf, P. O'Brien, G. Z. Mashanovich, and M. Nedeljkovic, *J. Opt.* **18**, 073003 (2016).
- ⁴B. Jalali and S. Fathpour, *J. Lightwave Technol.* **24**, 4600 (2006).
- ⁵M. Tang, J. S. Park, Z. Wang, S. Chen, P. Jurczak, A. Seeds, and H. Liu, *Prog. Quantum Electron.* **66**, 1 (2019).
- ⁶R. Won, *Nat. Photonics* **4**, 498 (2010).
- ⁷D. Liang and J. E. Bowers, *Nat. Photonics* **4**, 511 (2010).
- ⁸A. E. J. Lim, J. Song, Q. Fang, C. Li, X. Tu, N. Duan, K. K. Chen, R. P. -C. Tern, and T. Y. Liow, *IEEE J. Sel. Top. Quantum Electron.* **20**, 405 (2013).
- ⁹J. M. Ramirez, H. Elfaiki, T. Verole, C. Besancon, A. Gallet, D. Néel, K. Hassan, S. Olivier, C. Jany, S. Malhouitre, K. Gradkowski, P. E. Morrissey, P. O'Brien, C. Caillaud, N. Vaissière, J. Decobert, S. Lei, R. Enright, A. Shen, and M. Achouche, *IEEE J. Sel. Top. Quantum Electron.* **26**, 1 (2020).
- ¹⁰T. Komljenovic, M. Davenport, J. Hulme, A. Y. Liu, C. T. Santis, A. Spott, S. Srinivasan, E. J. Stanton, C. Zhang, and J. E. Bowers, *J. Lightwave Technol.* **34**, 20 (2016).
- ¹¹Y. Han, Y. Xue, Z. Yan, and K. M. Lau, *J. Lightwave Technol.* **39**, 940 (2021).
- ¹²W. Luo, Y. Xue, J. Huang, L. Lin, B. Shi, and K. M. Lau, *Photonics Res.* **8**, 1888 (2020).
- ¹³Y. Xue, W. Luo, S. Zhu, L. Lin, B. Shi, and K. M. Lau, *Opt. Express* **28**, 18172 (2020).
- ¹⁴Y. Wan, J. Norman, Q. Li, M. J. Kennedy, D. Liang, C. Zhang, D. Huang, Z. Zhang, A. Y. Liu, A. Torres, D. Jung, A. C. Gossard, E. L. Hu, K. M. Lau, and J. E. Bowers, *Optica* **4**, 940 (2017).
- ¹⁵S. Chen, J. Wu, W. Li, M. Liao, M. Tang, Q. Jiang, S. Shutts, S. Elliott, A. Sobiesierski, I. Ross, P. Snowton, A. Seeds, and H. Liu, in *2016 International Semiconductor Laser Conference (ISLC)* (IEEE, 2016), pp. 1–2.
- ¹⁶B. Kunert, Y. Mols, M. Baryshnikova, N. Waldron, A. Schulze, and R. Langer, *Semicond. Sci. Technol.* **33**, 093002 (2018).
- ¹⁷Y. Han, Y. Xue, and K. M. Lau, *Appl. Phys. Lett.* **114**, 192105 (2019).

- ¹⁸M. Baryshnikova, Y. Mols, Y. Ishii, R. Alcotte, H. Han, T. Hantschel, O. Richard, M. Pantouvak, J. Van Campenhout, D. Van Thourhout, R. Langer, and B. Kunert, *Crystals* **10**, 330 (2020).
- ¹⁹J. Z. Li, J. Bai, J. S. Park, B. Adekore, K. Fox, M. Carroll, A. Lochtefeld, and Z. Shellenbarger, *Appl. Phys. Lett.* **91**, 021114 (2007).
- ²⁰C. Merckling, N. Waldron, S. Jiang, W. Guo, N. Collaert, M. Caymax, E. Vancoille, K. Barla, A. Thean, M. Heyns, and W. Vandervorst, *J. Appl. Phys.* **115**, 023710 (2014).
- ²¹B. Kunert, W. Guo, Y. Mols, B. Tian, Z. Wang, Y. Shi, D. Van Thourhout, M. Pantouvaki, J. Van Campenhout, R. Langer, and K. Barla, *Appl. Phys. Lett.* **109**, 091101 (2016).
- ²²T. Orzali, A. Vert, B. O'Brian, J. L. Herman, S. Vivekanand, S. S. Papa Rao, and S. R. Oktyabrsky, *J. Appl. Phys.* **120**, 085308 (2016).
- ²³B. F. Mayer, S. Wirths, S. Mauthe, P. Staudinger, M. Sousa, J. Winiger, H. Schmid, and K. E. Moselund, *IEEE Photonics Technol. Lett.* **31**, 1021 (2019).
- ²⁴H. Schmid, M. Borg, K. Moselund, L. Gignac, C. M. Breslin, J. Bruley, D. Cutaia, and H. Riel, *Appl. Phys. Lett.* **106**, 233101 (2015).
- ²⁵F. Zhang, X. Zhang, Z. Li, R. Yi, Z. Li, N. Wang, X. Xu, Z. Azimi, L. Li, M. Lysevych, X. Gan, Y. Lu, H. Hoe Tan, C. Jagadish, and L. Fu, *Adv. Funct. Mater.* **32**, 2103057 (2022).
- ²⁶Y. Han, W. K. Ng, C. Ma, Q. Li, S. Zhu, C. C. S. Chan, K. W. Ng, S. Lennon, R. A. Taylor, K. S. Wong, and K. M. Lau, *Optica* **5**, 918 (2018).
- ²⁷Y. Li, W. Yang, S. Du, X. Zhou, M. Wang, H. Yu, Y. Zhang, and J. Pan, in *2019 International Photonics and Optoelectronics Meeting (OFDA, OEDI, ISST, PE, LST, TSA)*, OSA Technical Digest (Optica Publishing Group, 2019), paper JTh4E.6.
- ²⁸Y. Han, Z. Yan, W. K. Ng, Y. Xue, K. S. Wong, and K. M. Lau, *Optica* **7**, 148 (2020).
- ²⁹Y. Han, W. K. Ng, Y. Xue, Q. Li, K. S. Wong, and K. M. Lau, *Opt. Lett.* **44**, 767 (2019).
- ³⁰S. Mauthe, Y. Baumgartner, M. Sousa, Q. Ding, M. D. Rossell, A. Schenk, L. Czornomaz, and K. E. Moselund, *Nat. Commun.* **11**, 1 (2020).
- ³¹Y. Xue, Y. Han, Y. Wang, Z. Zhang, H. K. Tsang, and K. M. Lau, *Opt. Lett.* **45**, 1754 (2020).
- ³²Z. Yan, Y. Han, L. Lin, Y. Xue, C. Ma, W. K. Ng, K. S. Wong, and K. M. Lau, *Light Sci. Appl.* **10**, 200 (2021).
- ³³J. Li, Y. Xue, L. Lin, Z. Xing, K. S. Wong, and K. M. Lau, *J. Lightwave Technol.* **40**, 5631 (2022).
- ³⁴Y. Xue, Y. Han, Y. Tong, Z. Yan, Y. Wang, Z. Zhang, H. K. Tsang, and K. M. Lau, *Optica* **8**, 1204 (2021).
- ³⁵Y. Xue, Y. Han, Y. Wang, J. Li, J. Wang, Z. Zhang, X. Cai, H. K. Tsang, and K. M. Lau, *Optica* **9**, 1219 (2022).
- ³⁶Q. Gao, D. Saxena, F. Wang, L. Fu, S. Mokkaapati, Y. Guo, L. Li, J. Wong-Leung, P. Caroff, H. H. Tan, and C. Jagadish, *Nano Lett.* **14**, 5206 (2014).
- ³⁷J. Lin, X. Zhao, D. A. Antoniadis, and J. A. del Alamo, *IEEE Electron Device Lett.* **35**, 440 (2014).
- ³⁸L. Cheng, J. Fan, D. Janssen, D. Guo, X. Chen, F. J. Towner, and F. S. Choa, *J. Electron. Mater.* **41**, 506 (2012).
- ³⁹M. Albrecht, S. Christiansen, J. Michler, W. Dorsch, H. P. Strunk, P. O. Hansson, and E. Bauser, *Appl. Phys. Lett.* **67**, 1232 (1995).
- ⁴⁰F. Jonsdottir and L. B. Freund, *MRS Online Proc. Libr.* **317** 309 (1993).
- ⁴¹F. Bugge, U. Zeimer, M. Sato, M. Weyers, and G. Tränkle, *J. Cryst. Growth* **183**, 511 (1998).
- ⁴²S. Lutgen, T. Marschner, W. Stolz, E. O. Göbel, and L. Tapfer, *J. Cryst. Growth* **152**, 1 (1995).
- ⁴³G. Brammertz, Y. Mols, S. Degroote, M. Leys, J. Van Steenberghe, G. Borghs, and M. Caymax, *J. Cryst. Growth* **297**, 204 (2006).
- ⁴⁴Y. Han, Z. Yan, Y. Xue, and K. M. Lau, *Appl. Phys. Lett.* **117**, 052102 (2020).
- ⁴⁵R. Nagarajan, M. Kato, J. Pleumeekers, P. Evans, S. Corzine, S. Hurtt, A. Dentai, S. Murthy, M. Missey, R. Muthiah, R. A. Salvatore, C. Joyner, R. Schneider, M. Ziari, F. Kish, and D. Welch, *IEEE J. Sel. Top. Quantum Electron.* **16**, 1113 (2010).
- ⁴⁶J. Klamkin, H. Zhao, B. Song, Y. Liu, B. Isaac, S. Pinna, F. Sang, and L. Coldren, in *2018 IEEE BiCMOS and Compound Semiconductor Integrated Circuits and Technology Symposium (BCICTS)* (IEEE, 2018), pp. 8–13.